Dendromesogens: Liquid Crystal Organizations of Poly(amidoamine) Dendrimers versus Starburst Structures**

Mercedes Marcos,[a] Raquel Giménez,[a] José Luis Serrano,*[a] Bertrand Donnio,[b] Benoit Heinrich,[b] and Daniel Guillon[b]

Dedicated to Professor José Barluenga on the occasion of his 60th birthday

Abstract: A new series of liquid crystalline poly(amidoamine) (PAMAM) dendrimers is described. These dendrimers are made by attaching to the 0-, 1-, 2-, 3-, and 4-generation of PAMAM-terminal promesogenic units that carry two decyloxy chains in the 3- and 4-positions of their peripheral aromatic ring. X-ray diffraction studies show that all the compounds display a hexagonal columnar mesophase. A high density of aliphatic chains imposes a curved interface with the promesogenic units that forces the molecules to adopt a radial conformation, and therefore, the columnar structure. A model for the supramolecular organization of the different generations within the columnar mesophase is proposed based on the variation of some of the structural parameters.

Keywords: dendrimers · dendromesogens · liquid crystals · supramolecular chemistry

Introduction

One of the most interesting aspects of polymer chemistry is the observation of how very weak intermolecular forces, mainly van der Waals forces or in some cases intermolecular hydrogen bonds, can determine the unique properties of these materials.[1] Dendrimeric compounds represent an optimum testing bench in these types of studies. In these covalent materials, the molecules are forced to adopt very constrained and regular structures, and consequently, the different molecular parts tend to look for the most favorable positions in order to obtain the most stable structure. In this way, it is possible to observe in dendrimeric materials a wide variety of different macromolecular structures that produce original supramolecular organizations in some cases and/or new and interesting properties in others.[2]

Among the different types of dendrimeric materials, the liquid crystal dendrimers or dendromesogens prove to be of special relevance for structure–activity relationship studies. In these compounds, the interaction between the different mesogenic units could modify to a great extent the molecular arrangement and consequently the type of mesophase observed.[3–17]

Liquid crystalline dendrimers are also of academic interest in that they combine two opposite tendencies: the structural anisotropic units and the isotropic dendritic architecture. Indeed, the branches radiate from a central core and become more crowded as they extend out to the periphery; this results in a spherical morphology (starburst shape in dendrimer terminology), that is, all branches tend to be isotropically distributed in space because of entropic forces. However, mesogenic groups show strong anisotropic interactions between them, which result in the formation of mesophases caused by the enthalpic gain. Therefore, this class of materials represents a nice example of the competition between entropy and enthalpy within one molecule.

We have recently reported the liquid crystalline properties of some poly(amidoamine) (PAMAM) dendrimers functionalized in their terminal groups by one-chain promesogenic calamitic units.[15] In these compounds, and in contrast to the starburst structure promoted by the PAMAM-only dendrimers, the weak interactions between the mesogenic units make the molecules adopt a cylindrical geometry, which resembles a heavy thick rodlike structure that induces smectic phases.

In this paper, we present the results obtained for a series of homologous PAMAM dendrimers that carry in the terminal

[a] Prof. J. L. Serrano, Dr. M. Marcos, Dr. R. Giménez
Química Orgánica, Facultad de Ciencias-ICMA
Universidad de Zaragoza-CSIC, 50009 Zaragoza (Spain)
Fax: (+34) 976-761209
E-mail: joseluis@posta.unizar.es

[b] Dr. B. Donnio, Dr. B. Heinrich, Dr. D. Guillon
Institut de Physique et Chimie
des Matériaux de Strasbourg
Groupe des Matériaux Organiques, 23, rue du Loess
67037 Strasbourg Cedex (France)

[**] Part 2; for Part 1 see: J. Barberá, M. Marcos, J. L. Serrano, *Chem. Eur. J.* **1999**, *5*, 1834.

0947-6539/01/0705-1006 $ 17.50+.50/0

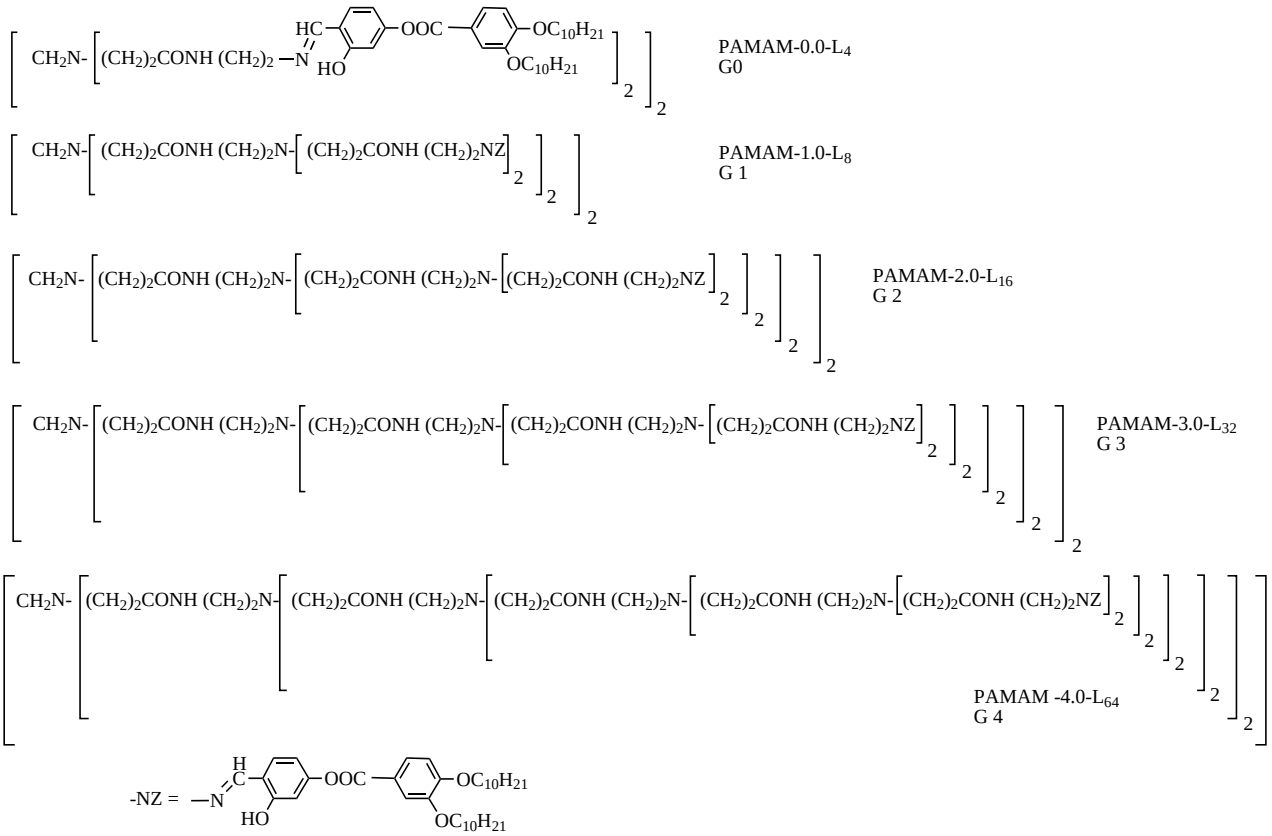

Scheme 1. Structure of the five generation dendrimers.

promesogenic units two decyloxy chains in the 3- and 4-positions of the peripheral aromatic ring (Scheme 1). This change modifies the relationship between the hard part of the dendrimer and the soft part, corresponding to the PAMAM central structure and the alkoxy-terminal chains, respectively. As a consequence of this additional terminal chain, the molecular interactions are modified, the formation of the aforementioned lamellar structure is then hindered, and the molecules adopt another conformation that induces columnar mesomorphism (Figure 1).

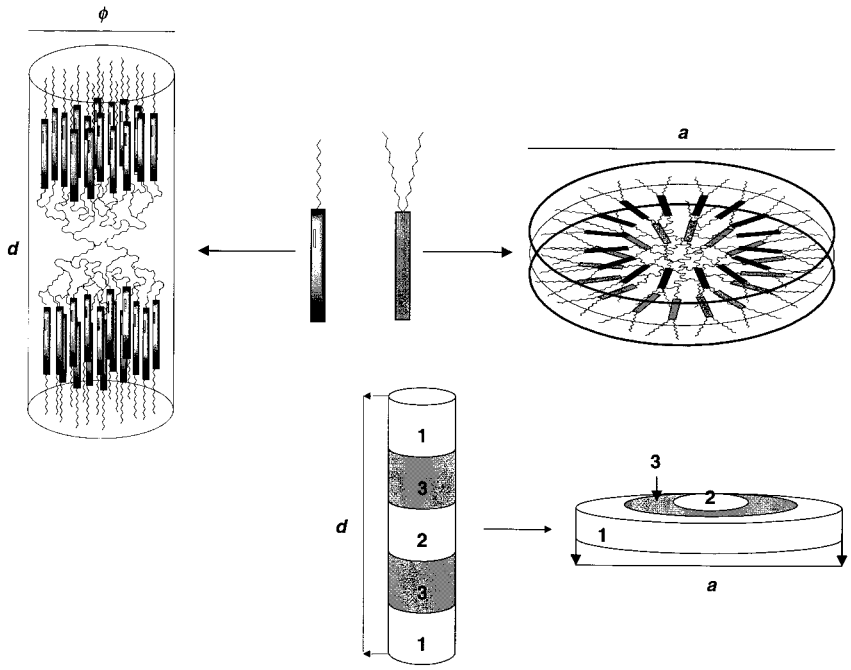

Figure 1. Giant rods versus giant discs. Soft parts of the dendrimer (white areas): 1) terminal alkyl chains, 2) central PAMAM groups; hard parts of the dendrimer (gray areas): 3) promesogenic units.

Results and Discussion

Synthesis and characterization: The dendrimers were synthesized by the condensation of 4-(3′,4′-didecyloxybenzoyloxy)-salicylaldehyde with the terminal amino groups of the corresponding generation of PAMAM (0, 1, 2, 3, and 4).[15] All the compounds were isolated as air-stable yellow solids, which are soluble in solvents such as dichloromethane, chloroform, and THF, and insoluble in ethanol.

The chemical structures of these compounds have been established by using ^{1}H, ^{13}C NMR, and IR spectroscopy,

  0947-6539/01/0705-1007 $ 17.50+.50/0

FAB^+ mass spectrometry, gel permeation chromatography (GPC), and elemental analysis. All the above techniques gave satisfactory results. These results are comparable to those obtained for the one-terminal chain calamitic homologues previously described.[15]

IR, ^1H, and ^{13}C NMR spectroscopy have proved very useful in confirming the structure and the purity of these materials. Evidence for the condensation reactions was provided by the lack of a signal at $\delta = 195$ in the ^{13}C NMR spectra (which corresponds to the carbonyl of the aldehyde) along with the total absence of the NH_2 signals from the starting compound in ^1H NMR and IR spectra. In addition, the excellent solubility of these dendrimers in $CDCl_3$ allowed us to integrate the different peaks in the ^1H NMR spectra, and this confirms in all cases that the expected polymers were obtained.

The molecular masses of the higher molecular weight dendrimers (PAMAM-2.0-L_{16}, PAMAM-3.0-L_{32}, and PAMAM-4.0-L_{64}) could not be measured by the FAB^+ technique. In contrast, the lower molecular weight dendrimers (PAMAM-0.0-L_4 and PAMAM-1.0-L_8) exhibit a FAB^+ spectrum that contains peaks for $[M+1]^+$ and $[M+Na]^+$ ions. GPC measurements (mobile phase: THF, calibration standard: polystyrene) confirmed in all cases, the presence of practically monodisperse polymers. However, as this is often the case with dendrimers, a deviation from the calculated molecular weight was found in the experimental data, even for the low molecular weight compounds.[18]

Mesomorphic properties: The liquid crystalline properties and the thermal stability of these compounds have been studied by polarizing optical microscopy, differential scanning calorimetry (DSC), thermogravimetry, and X-ray diffraction (XRD). The thermal and thermodynamic data are summarized in Table 1.

All the dendrimers prepared show liquid crystalline behavior. Under the optical microscope a mesophase appears in all cases. The texture of the mesophase displayed by these compounds does not show any characteristic features, although in some cases a pseudo-focal-conic texture was identified.

Thermogravimetric analysis shows that all dendrimers remain without any loss of weight below the clearing temperature (T_i), as can be seen in the data of Table 1. As for the related homologous compounds previously described, these dendrimers behave as normal polymers, and, in general, the DSC curves for the first heating scan show the T_m (melting transition) and the T_i clearly. However, very simple thermograms were obtained, and the glass transition temperature (T_g) could be observed in the second heating scan after an annealing process. The T_i temperature could not be clearly detected (see Table 1), except for the PAMAM-3.0-L_{32} (in the second heating scan). The mesophases freeze at low temperature, and it is not possible to observe the crystallization peak, even at $-20\,^\circ C$.

For the first three generations of dendrimers, two peaks were detected. These peaks probably correspond to two different crystalline phase transitions. Surprisingly, the temperature range of the crystalline form that appears at higher temperatures increases with the dendrimer size.

The enthalpies of the crystal-to-mesophase and mesophase-to-isotropic liquid transitions show very similar values when the data are normalized to the number of promesogenic units of each dendrimer. These values are around 21 kJ at T_m and 0.4 kJ at T_i, and this indicates that all the dendrimers show an identical thermal behavior.

X-ray diffraction studies: Temperature-dependent X-ray diffraction experiments were carried out for the whole series of compounds in order to characterize the mesophase observed by polarizing optical microscopy and by DSC. The X-ray patterns, obtained in the temperature range given in Table 1, are qualitatively similar in all cases and are typical of the hexagonal columnar mesophase, Col_H. A diffuse scattering halo in the wide-angle region centered at around 4.5 Å, corresponding to the liquidlike disorder of the molten chains, confirmed the liquid crystalline nature of the mesophase. Up to three and sometimes four sharp small-angle reflections, corresponding to the reciprocal spacings in the ratios 1, $\sqrt{3}$, $\sqrt{4}$, and $\sqrt{7}$, and to the indexation $(hk) = (10)$, (11), (20), and (21), were observed in the patterns, indicative of a two-dimensional hexagonal packing of the columns. In Table 2, some of the main structural parameters of the mesophase are

Table 1. Thermal and thermodynamic data for dendrimers.

	TG [°C][a]	Mesophase	T_g [°C][b]	T_m [°C][c]	ΔH_{Tm} [KJ mol^{-1}]	ΔH_{Tm} [JP.u.][d]	T_i [°C]	ΔH_{Ti} [KJ mol^{-1}]	ΔH_{Ti} [JP.u.]
PAMAM-0.0-L_4	175	Col_H	32	61.9 80.1	83.5 2.9 } 86.4	20.9 0.4 } 21.3	138.9	1.6	0.4
PAMAM-1.0-L_8	200	Col_H	45	64.2 117.8	160.1 28.6 } 188.7	20.0 3.6 } 23.6	162.2	2.3	0.3
PAMAM-2.0-L_{16}	210	Col_H	47	58.3 121.1	71.0 268.5 } 339.5	4.4 16.8 } 21.2	188.2	7.1	0.4
PAMAM-3.0-L_{32}[e]	200	Col_H	29	63.8	727.6	22.7	188.9 210[e]	13.9 13.8[e]	0.4 0.4[e]
PAMAM-4.0-L_{64}	210	Col_H	30	52.5	1367.7	21.4	199.0	29.1	0.4

[a] Starting temperature of the loss of weight (onset). [b] The glass transition temperature has been measured in the second heating process. [c] First heating scan for compounds PAMAM-0.0-L_4, PAMAM-1.0-L_8, and PAMAM-2.0-L_{16}; the two C-M transitions have been detected. [d] Transition enthalpy normalized to one promesogenic unit. [e] Data corresponding to the second heating scan. Only for compound PAMAM-3.0-L_{32} has a T_i been detected in the second heating scan.

0947-6539/01/0705-1008 $ 17.50+.50/0 *Chem. Eur. J.* **2001**, *7*, No. 5

Table 2. Structural parameters of the Col_H mesophase as a function of generation number (GN) and temperature (T): d_{10} is first-order spacing and s is columnar cross section.

GN	$T=80\,^{\circ}C$		$T=100\,^{\circ}C$		$T=120\,^{\circ}C$	
	d_{10} [Å]	s [Å^2]	d_{10} [Å]	s [Å^2]	d_{10} [Å]	s [Å^2]
G0	49.2	2794	46.8	2527	–	–
G1	56.7	3711	52.5	3178	52.0	3126
G2	53.6	3320	51.5	3065	53.1	3258
G3	60.9	4280	58.2	3912	55.2	3519
G4	56.0	3620	54.9	3483	53.2	3275

collected as a function of generation number and temperature.

Supramolecular organization in the mesophase: As it can be seen from the results presented in Tables 1 and 2, all the compounds show a Col_H phase. However, as explained above, in the case of the homologous dendrimers with only one terminal chain in the promesogenic unit, only a SmA (smectic A) phase was observed.

The grafting of two terminal chains avoids the parallel disposition of the promesogenic units to produce a smectic phase and instead forces the molecule to adopt a radial conformation. In this case, the mesogenic units are radially arranged around a central moiety to which they are linked by a variable number of amidoamine units that extend from the molecule center (Figure 1). The columnar mesophase results from the stacking of the molecules in their radial conformation as sketched in Figure 2; the formation of such layer–block dendrimeric structures is driven by microphase separation between the incompatible segments of the molecule (the curly arrangement of the amidoamine units, the concentric rigid aromatic belt, and the peripheral soft crown).[19]

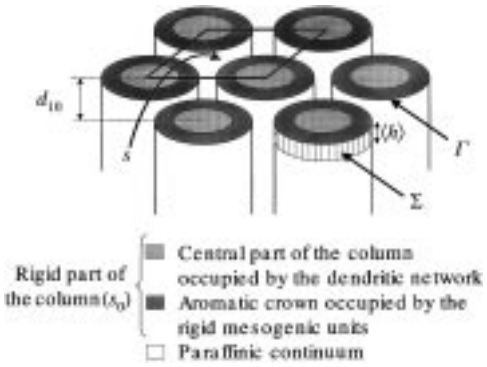

Figure 2. Location of the different partial volumes associated with the different parts of the molecules, which are packed in columns in the hexagonal mode. Visualization of the different structural parameters discussed in the text: s, Σ, Γ, $\langle h \rangle$, and d_{10}.

Packing study: In order to understand the molecular arrangement of the different generations within the columnar mesophase, the variation of some structural parameters was analyzed as a function of both the temperature and the generation number, namely the cross-sectional area of the column, s, and the volumes of the different segments of the dendrimers. Our methodology consisted of determining the number of aliphatic chains that radiate out from a slice of column, and thus to calculate the number of molecules within this slice. The thickness of the columnar slice, $\langle h \rangle$, corresponds to the repeating unit distance along the columnar axis. In order to achieve this objective, we based our analysis on a simple additivity rule for the calculation of the specific volumes (which has been proved correct in many cases to date[20]). We also needed to define the cross-sectional area of the inner rigid part of the column, s_0, and the thickness of a columnar slice, $\langle h \rangle$. These parameters are obtained experimentally (dilatometry and XRD). $\langle h \rangle$ is determined in the wide-angle area of the diffraction pattern; however due to a poor experimental resolution (diffuse halo), it has to be determined analytically (see also Figure 2 for the visualization of these parameters).

If we consider the molecule in its radial conformation (see above), its different segments were identified on the basis of their amphipatic character,[19] and the following parts were differentiated as follows: a *branching* part, that is, the central dendrimeric network, a *hard-core* part, that is, the concentric central rigid part formed by the aromatic cores of the promesogenic units, and finally, a *chain* part, that is, the terminal alkoxy chains. These three different parts are characterized by three volumes, V_{br} (branching part volume), V_{ar} (hard-core part volume), and V_{ch} (aliphatic chain part volume), which are calculated separately as a function of temperature. The molecular volume, V_m, can thus be written as a sum of elementary volumes [Eq. (1)].

$$V_m = V_{br} + V_{ar} + V_{ch} \quad (1)$$

In Equation (1), V_{br}, V_{ar}, and V_{ch} are obtained from density measurements of the elementary constitutive units $V_{br} = (M_{br}/M_{CH2})v_{CH2}$, $V_{ar} = (M_{ar}/m_{ar})v_{ar}$, and $V_{ch} = (M_{ch}/M_{CH2})v_{CH2}$. M_{br}, M_{ar}, and M_{ch} are the molecular weights of the different parts of the molecule, respectively, m_{ar} is the molecular weight of one mesogenic unit's rigid part ($m_{ar} = 270.22\ g\,mol^{-1}$) and v_{ar} is its volume ($v_{ar} = 340$ Å^3 from dilatometry experiments), $M_{CH2} = 14.01\ g\,mol^{-1}$, and v_{CH2} is the volume of one methylene group ($v_{CH2} = 26.56 + 0.02T$, with T in °C, obtained from dilatometric measurements on liquid paraffin).[21] Note that the density of the central dendritic network was taken to be equal to the density of a paraffinic chain.

The volume fraction of the central core of the column, χ, is thus equal to the volume fraction of the dendritic and aromatic constitutive parts of the molecule and is expressed in Equation (2).

$$\chi = \frac{V_{br} + V_{ar}}{V_m} \quad (2)$$

It is now possible to calculate s_0 (Figure 2), which corresponds to a percentage of s (equal to the dimension of the elementary cell of the hexagonal lattice, Figure 2) [Eq. (3)].

$$s_0 = s\chi = \frac{2}{\sqrt{3}}\chi d_{10}^2 \quad (3)$$

One can now calculate the corresponding perimeter of s_0, Γ. From the relationships between circle area and circle perimeter, the following expression is obtained [Eq. (4)].

$$\Gamma = 2\sqrt{\pi\chi s} \quad (4)$$

From geometric constraints, the minimum average distance between aliphatic chains occurs when they are fully stretched and projected radially from the interface. Thus, $\langle h \rangle$ can be estimated on the assumption that the cross-sectional area of one fully stretched, aliphatic chain, σ, is associated to a domain of influence known as the Wigner–Seitz cell (Figure 6),[22, 23] that is, a domain of a particular lattice point that consists of all points in space, which are closer to this lattice point than to any other lattice point. The value σ is the volume of one methylene group divided by the length of this group in the crystallized chain [$\sigma = (v_{CH2}/1.27)$]. The mean average distance, or thickness of a slice is $\langle h \rangle = g\sqrt{\sigma}$ (see Appendix), and the area of a interface of thickness $\langle h \rangle$ (the radial area of the slice), Σ (which is cylindrical because of the symmetry of the Col_H mesophase), is expressed in Equation (5).

$$\Sigma = \Gamma\langle h \rangle = 2\sqrt{\pi\chi s}\; g\sqrt{\sigma} = 2g\sqrt{\pi\chi s\sigma} \quad (5)$$

The number of chains, N_{ch}, as well as the number of molecules, N_{mol}, which can be accommodated within a columnar slice of the corresponding thickness $\langle h \rangle$ can thus be estimated according to the following equations [Eqs. (6a) and (6b)].

$$N_{ch} = \frac{\Sigma}{\sigma} = 2g\sqrt{\frac{\pi\chi s}{\sigma}} \quad (6a)$$

$$N_{mol} = \frac{N_{ch}}{2^{N_G+3}} \quad (6b)$$

In Equation (6b), N_G is the generation number ($N_G = 0-4$). The results of these calculations are reported in Table 3. It appears that, for the molecules G1 to G4, between 30 and 36 chains per columnar slice (4.6 Å thick) radiate from the cores; the exception is G0 where this number is smaller (26–27 chains). In this case, the lateral extension of the dendritic network is limited by the length of the branches and not by the bulkiness of the terminal aliphatic chains as in the higher generations. In the plot in Figure 3, the number of molecules per slice of column (repeat unit) is shown at different temperatures and compared with a theoretical curve fitted with a fixed value of $N_{ch} = 32$ chains for every generation (corresponding to one G2 molecule) per repeat unit (dotted line).

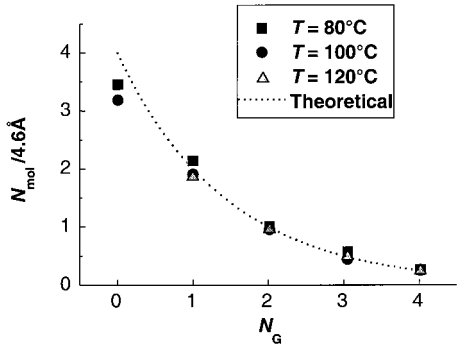

Figure 3. Number of molecules versus generation number.

Model: As can be deduced from the data of Tables 2 and 3, and from Figure 3, more than three molecules of the dendrimer of the generation 0 (G0) are needed to fill one columnar slice. In the case of the G1, two molecules are necessary to carry out this function. In Figure 4, two theoretical models of molecular arrangements are represented for each of these generations. Models 1 and 2 are two of the many possibilities for arrangements of the molecules in G0 or G1, and although they are not the only ones, they should contribute to some degree. Evidently, this is not a static system, and diffusion from one slice to another may also occur; this gives many other intermediate possibilities. In the G2, a unique molecule is able to fill the "disc", and in G3 and

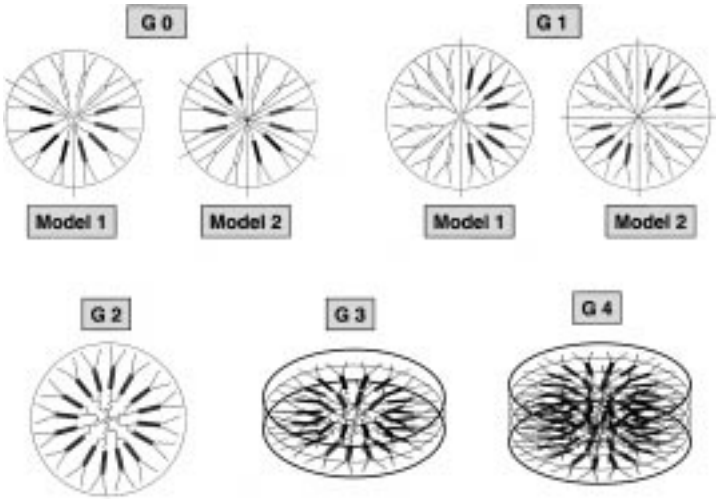

Figure 4. Packing mode of the dendrimeric molecules for every generation.

Table 3. Characteristics of the Col_H mesophase as a function of generation number (GN) and temperature (T): N^*_{mol} is the theoretical number of molecules per columnar slice (4.6 Å thick), χ the volume fraction, N_{ch} the number of chains, and N_{mol} the number of molecules per columnar slice (4.6 Å thick).

GN	Calcd	$T = 80\,^\circ C$			$T = 100\,^\circ C$			$T = 120\,^\circ C$		
	N^*_{mol}	χ	N_{ch}	N_{mol}	χ	N_{ch}	N_{mol}	χ	N_{ch}	N_{mol}
G0	4	0.50	27.5	3.4	0.50	26	3.2	–	–	–
G1	2	0.54	33	2.05	0.54	30	1.9	0.54	30	1.9
G2	1	0.56	32	1.0	0.56	30	1.0	0.54	30	0.9
G3	0.5	0.57	36	0.55	0.56	34	0.5	0.056	32	0.5
G4	0.25	0.57	33	0.25	0.57	32	0.25	0.57	31	0.25

0947-6539/01/0705-1010 $ 17.50+.50/0 *Chem. Eur. J.* **2001**, *7*, No. 5

G4 the molecular size is so enormous that more than one slice is needed in order to accommodate these molecules in the columns. Thus, two and four "discs" are necessary for the molecules of the G3 and G4 generation, respectively.

The general model that could explain the columnar mesophase is represented in Figure 5. The molecules of the five generations are arranged in cylindrical columns, in which

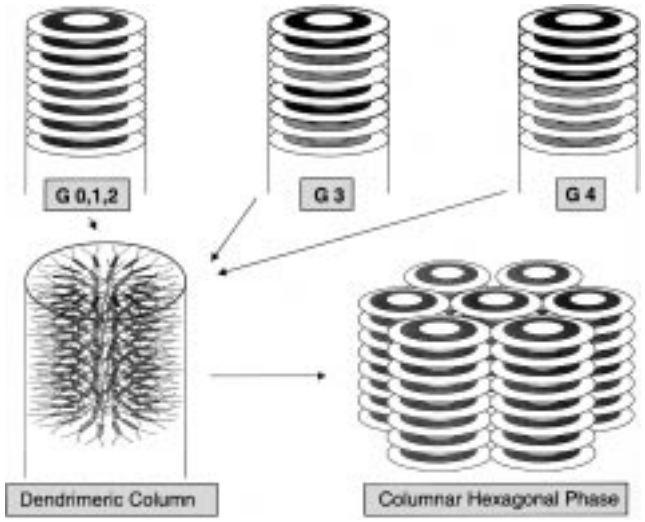

Figure 5. Supramolecular organization of the dendrimers within the columnar mesophase.

the molecules can have several conformations. These columns interact to form a columnar hexagonal phase similar to the lyotropic middle phases formed by micelle aggregations.[24] The formation of intra- and intermolecular hydrogen bonds between the amido groups helps to maintain a stable aggregation of the central structure, which plays a crucial role in the behavior of the PAMAM central group. The existence of these hydrogen bonds has been proved by means of spectroscopic methods, like IR and ^{1}H NMR spectroscopy.[14]

The most important trend of these systems is the very small variation of the intercolumnar spacings, d_{10}, as a function of the generation number (Table 2). It is worth pointing out that despite the exponential increase of the dendrimers' molecular weights, the columnar spacing variations are in between 6 and 8 Å, and only 3 Å at 120 °C. This clearly means that the volume expansion of the dendrimers occurs mainly in one direction, which is the direction parallel to the columnar axis. The other secondary variation of d_{10} as a function of temperature may be related to the variation of the tilt angle of the mesogenic subunits with respect to the columnar axis and/or to the plane of the hexagonal lattice in order to satisfy both molecular conformation and geometric constraints; this is in comparison with the purely radiative arrangement as shown in Figures 1 and 4.

Conclusion

We have shown in this paper that we have been able to produce columnar mesophases with dendrimers of high molecular weight. This has been achieved through proper chemical design, combined with the role of different types of intermolecular interactions. Hydrogen bonds between the amido groups contribute to a rather rigid internal core, which is always necessary for the formation of columnar mesophases.[25] The interactions between the polarizable promesogenic units combined with microsegregation effects contribute also to the stabilization of the columnar core. Finally, a high density of aliphatic chains imposes a curved interface with the promesogenic units, and therefore, the columnar structure. These disordered chains ensure at the same time the gliding of the columns, one with respect to the other, and thus the fluidity and the liquid crystalline nature of the phase.

Experimental Section

Techniques: Microanalyses were performed with a Perkin Elmer 240B microanalyzer. Infrared spectra were obtained with a Perkin Elmer 1600 (FTIR) spectrophotometer in the spectral range $\tilde{\nu} = 400 - 4000\ cm^{-1}$. ^{1}H and ^{13}C NMR spectra were recorded on a Varian Unity spectrometer (300 MHz) in solutions in $CDCl_3$. Mass spectra were obtained with a VG Autospec spectrometer with positive ion FAB (FAB^+). Gel permeation chromatography (GPC) was carried out in a Waters liquid chromatography system equipped with a 600E multisolvent delivery system and 996 photodiode array detector. Two Ultrastyragel columns (Waters; pore size 500–10^4 Å) were connected in series. THF was used as the mobile phase with a flow rate of 0.8 mL min^{-1}. Calibration was performed with polystyrene standards. The optical textures of the mesophases were studied with a Nikon polarizing microscope equipped with a Mettler FP8 hot-stage and an FP80 central processor. The transition temperatures and enthalpies were measured by differential scanning calorimetry with a Perkin Elmer DSC-7 instrument operated at a scanning rate of 10 °C min^{-1} on heating. The apparatus was calibrated with indium (156.6 °C; 28.4 J g^{-1}) as the standard. The XRD patterns were obtained with two different experimental setups; in all cases, the crude powder was filled in Lindemann capillaries (diameter: 1 mm). For the characterization of the wide-angle region, a linear monochromatic $Cu_{K\alpha 1}$ beam obtained with a sealed-tube generator (900 W) and a bent quartz monochromator was used. The diffraction patterns were registered with a curved counter Inel CPS 120. Periodicities up to 60 Å could be measured, and the sample temperature was controlled within ± 0.05 °C. The measurements of the periodicities were performed by using a linear monochromatic $Cu_{K\alpha 1}$ beam obtained with a sealed-tube generator (900 W) and a bent quartz monochromator. The diffraction patterns were registered on films; the cell parameters were calculated from the position of the reflection at the smallest Bragg angle, which was in all cases the most intense. Periodicities up to 90 Å could be measured, and the sample temperature was controlled within ± 0.3 °C. In each case, exposure times were varied from 1 to 24 h; the time depended on the compound under observation and upon the specific reflections that were sought (weaker reflections clearly have longer exposure times).

General procedure for the condensation of 4-(3′,4′-decyloxybenzoyloxy)-salicylaldehyde with PAMAM dendrimers: Neutral activated grade I alumina (0.5 g) and then the corresponding poly(amidoamine) were added to a stirred solution of 4-(3′,4′-decyloxybenzoyloxy)salicylaldehyde in dichloromethane (15 mL). The mixture was refluxed under nitrogen until the aldehyde had completely reacted (usually after eight to ten hours). The alumina was filtered off, and the solvent from the filtrate evaporated under vacuum. The resulting solid was dissolved in hexane and precipitated in ethanol. Yields were 70–85 %.

Characterization: Due to the similarity of the ^{1}H and ^{13}C NMR spectra of these materials, we only quoted these data for the PAMAM-2.0-L_{16} dendrimer as a representative example. The data obtained from other techniques have been quoted for all compounds.

PAMAM-0.0-L_4: IR (Nujol): $\tilde{\nu} = 3289$, 3075 (CON–H), 1727 (OC=O), 1656 (sh, OC–NH), 1637 cm^{-1} (CH=N); elemental analysis calcd (%) for $C_{158}H_{240}N_{10}O_{24}$: C 71.28, H 9.02, N 5.56; found C 71.6, H 8.6, N 5.3; FAB-MS (NBA matrix): m/z (%): 2684 $[M+Na]^+$.

PAMAM-1.0-L_8: IR (Nujol): $\tilde{\nu}$ = 3280, 3076 (CON−H), 1728 (OC=O), 1656 (sh, OC−NH), 1635 cm^{-1} (CH=N); elemental analysis calcd (%) for $C_{334}H_{512}N_{26}O_{52}$: C 70.11, H 8.97, N 6.36; found C 70.0, H 8.5, N 6.5; FAB-MS (NBA matrix): *m*/*z* (%): 5717 $[M+1]^+$.

PAMAM-2.0-L_{16}: ^{1}H NMR (300 MHz, RT, $CDCl_3$): δ = 13.7 (s, 1H), 8.22 (s, 1H), 7.89 (br s, 1H), 7.70 (d, J = 9 Hz, 1H), 7.57 (s, 1H), 7.13 (d, J = 9 Hz, 1H), 6.85 (d, J = 9 Hz, 1H), 6.65 (s, 1H), 6.57 (d, J = 9 Hz, 1H), 4.00 (t, 4H), 3.64 (br s, 2H), 3.47 (br s, 2H), 3.20 (br s, 2H), 2.68 (br s, 2H), 2.48 (br s, 2H), 2.30 (br s, 2H), 1.80 (m, 4H), 1.44 (m, 4H), 1.24 (s, 32H), 0.84 (t, 6H); ^{13}C NMR (300 MHz, RT, $CDCl_3$): δ = 173.16, 172.67, 165.83, 164.65, 164.19, 154.69, 154.05, 148.74, 132.79, 124.54, 121.19, 116.27, 114.65, 112.12, 111.98, 110.77, 77.49, 77.07, 76.65, 69.39, 69.07, 57.29, 52.37, 50.12, 40.04, 37.38, 34.04, 31.91, 29.61, 29.58, 29.44, 29.42, 29.35, 29.23, 29.09, 26.05, 25.99, 22.67, 14.09; IR (Nujol): $\tilde{\nu}$ = 3286, 3076 (CON−H), 1728 (OC=O), 1659 (sh, OC−NH), 1633 cm^{-1} (CH=N); elemental analysis calcd (%) for $C_{686}H_{1056}N_{58}O_{108}$: C 69.60, H 9.52, N 6.86; found C 69.3, H 8.5, N 6.9.

PAMAM-3.0-L_{32}: IR (Nujol): $\tilde{\nu}$ = 3285, 3076 (CON−H), 1728 (OC=O), 1658 (sh, OC−NH), 1639 cm^{-1} (CH=N); elemental analysis calcd (%) for $C_{1390}H_{2144}N_{122}O_{220}$: C 71.98, H 9.25, N 7.31; found C 72.0, H 9.1, N 7.3.

PAMAM-4.0-L_{64}: IR (Nujol): $\tilde{\nu}$ = 3276, 3078 (CON−H), 1726 (OC=O), 1656 (sh, OC−NH), 1635 cm^{-1} (CH=N); elemental analysis calcd (%) for $C_{2798}H_{4320}N_{250}O_{444}$: C 69.22, H 8.90, N 7.21; found C 69.0, H 8.8, N 7.2.

Appendix

Calculation of $\langle h \rangle$ and g[26]: In order to estimate $\langle h \rangle$, the mean average distance between two closest adjacent chains, which also represents the thickness of the repeating columnar slices along the columnar axis, we considered an aliphatic/aromatic interface. The chains radiate normally from this interface (at least in its vicinity), and they are densely packed according to a hexagonal mode (maximum packing). Therefore, at the interface, by using the cell of a hexagonal Wigner–Seitz lattice, it is possible to calculate $\langle h \rangle$, which varies between h_{min} and h_{max}; h_{min} is the shortest distance between two chains, and h_{max} is the largest distance (Figure 6). From Figure 6, the following expression can be obtained [Eq. (7)].

$$\frac{h_{max}}{h_{min}} = \frac{1}{\cos 30} = \frac{2}{\sqrt{3}} \tag{7}$$

Thus Equation (8) can be obtained, in which θ is the angle between h and h_{min}.

$$\frac{h}{h_{min}} = \frac{1}{\cos\theta} \tag{8}$$

Therefore the mean average ratio, $\langle (h/h_{min} \rangle$, is given by the following integration [Eq. (9)].

$$\left\langle \frac{h}{h_{min}} \right\rangle = \frac{1}{\theta_2 - \theta_1} \int_{\theta_1}^{\theta_2} \frac{d\theta}{\cos\theta} \tag{9}$$

For symmetry reasons, the average ratio can be integrated between θ_1 (0°) and θ_2 (30°), and thus Equation (10) is obtained.

$$\left\langle \frac{h}{h_{min}} \right\rangle = \frac{3}{\pi} \log 3 \tag{10}$$

The area of the hexagonal Wigner–Seitz lattice, σ, is defined by:

$$\sigma = h_{min} \times h_{max} = \frac{2}{\sqrt{3}} h_{min}^2 \tag{11a}$$

and h_{min} is deduced directly

$$h_{min} = \sqrt{\frac{\sigma\sqrt{3}}{2}} \tag{11b}$$

Thus Equation (12a) is obtained by replacing (11b) in (10).

$$\langle h \rangle = \sqrt{\sigma}\, \frac{3^{\frac{5}{4}}}{\pi\sqrt{2}} \mathrm{Log} 3 = g\sqrt{\sigma} \tag{12a}$$

and

$$\langle h \rangle = 0.9763\sqrt{\sigma} \tag{12b}$$

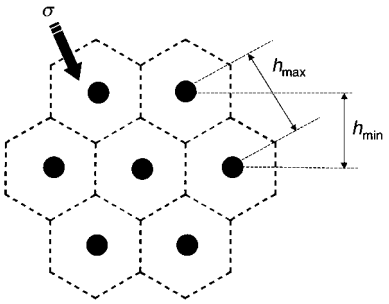

Figure 6. Representation of the hexagonal cell of the Wigner–Seitz lattice (dotted lines), located on the interface Σ. Black circles: anchoring points of the aliphatic chains.

Acknowledgements

This work was supported by the Comisión Interministerial de Ciencia y Tecnología (project MAT97-0986-C02-01), the European Union (FMRX CT97 0121), and the French-Spanish cooperation program (Picasso 99162).

[1] F. W. Billmeyer, Jr., *Textbook of Polymer Science*, 3rd ed., Wiley, New York, **1984**, Chapter 1, p. 11; (Molecular forces and chemical bonding in polymers).

[2] a) G. R. Newkome, C. N. Moorefield, F. Vögtle, *Dendritic Molecules: Concepts, Synthesis and Perspectives*, VCH, Weinheim, **1996**; b) D. A. Tomalia, A. M. Naylor, W. A. Goddard III, *Angew. Chem.* **1990**, *102*, 119; *Angew. Chem. Int. Ed. Engl.* **1990**, *29*, 138; c) O. A. Matthews, A. N. Shipway, J. F. Stoddart, *Prog. Polym. Sci.* **1998**, *23*, 1; d) F. W. Billmeyer, Jr., *Textbook of Polymer Science*, 3rd ed., Wiley, New York, **1984**, Chapter 1, p. 241; e) P. R. Ashton, S. E. Boyd, C. L. Brown, S. A. Nepogodiev, E. W. Meijer, H. W. I. Peerlings, J. F. Stoddart, *Chem. Eur. J.* **1997**, *3*, 974; f) H. F. Chow, T. K. K. Mong, M. F. Nongrum, C. W. Wan, *Tetrahedron* **1998**, *54*, 8543; g) N. Ardouin, D. Astruc, *Bull. Soc. Chem. Fr.* **1995**, *132*, 875.

[3] J. H. Cameron, A. Facher, G. Latterman, S. Diele, *Adv. Mater.* **1997**, *9*, 398.

[4] S. E. Friberg, M. Podzimek, D. A. Tomalia, D. M. Hedstrand, *Mol. Cryst. Liq. Cryst.* **1988**, *164*, 157.

[5] S. Bauer, H. Fischer, H. Ringsdorf, *Angew. Chem.* **1993**, *105*, 1658; *Angew. Chem. Int. Ed. Engl.* **1993**, *32*, 1589.

[6] a) V. Percec, M. Kawasumi, *Macromolecules* **1992**, *25*, 3843; b) V. Percec, P. Chu, M. Kawasumi, *Macromolecules* **1994**, *27*, 4441; c) V. Percec, P. Chu, G. Ungar, J. Zhou, *J. Am. Chem. Soc.* **1995**, *117*, 11441; d) V. S. K. Balagurusamy, G. Ungar, V. Percec, G. Johansson, *J. Am. Chem. Soc.* **1997**, *119*, 1539; e) S. D. Hudson, H. T. Jung, V. Percec, W. D. Cho, G. Johansson, G. Ungar, U. S. K. Balagurusamy, *Science* **1997**, *278*, 449; f) V. Percec, W. D. Cho, P. E. Mosier, G. Ungar, D. J. P. Yeardley, *J. Am. Chem. Soc.* **1998**, *120*, 11061; g) S. D. Hudson, H. T. Jung, P. Kewsuwan, V. Percec, W. D. Cho, *Liq. Cryst.* **1999**, *26*, 1493.

[7] a) S. A. Ponomarenko, E. A. Rebrov, A. Y. Bobronsky, N. I. Boiko, A. M. Mugafarov, V. P. Shibaev, *Liq. Cryst.* **1996**, *21*, 1; b) K. Lorenz, D. Hölter, R. Mühlhaupt, H. Frey, *Adv. Mater.* **1996**, *8*, 414.

[8] a) D. J. Pesak, J. S. Moore, *Angew. Chem.* **1997**, *109*, 1709; *Angew. Chem. Int. Ed. Engl.* **1997**, *36*, 1636; b) H. Meier, M. Lehmann, *Angew. Chem.* **1998**, *110*, 666; *Angew. Chem. Int. Ed.* **1998**, *37*, 643; c) H. Meier, M. Lehmann, U. Kolb, *Chem. Eur. J.* **2000**, *6*, 2462; d) M. Lehmann, B. Schartel, M. Hennecke, H. Meier, *Tetrahedron* **1999**, *55*, 13377.

[9] M. W. P. L. Baars, S. H. M. Söntjens, H. M. Fischer, H. W. I. Peerlings, E. W. Meijer, *Chem. Eur. J.* **1998**, *4*, 2456.

[10] P. Busson, H. Ihre, A. Hult, *J. Am. Chem. Soc.* **1998**, *120*, 9070.

[11] R. M. Richardson, S. A. Ponomarenko, N. I. Boiko, V. P. Shivaev, *Liq. Cryst.* **1999**, *26*, 101.

[12] K. Yonetake, T. Masuko, T. Morishita, K. Suzuki, M. Ueda, R. Nagahata, *Macromolecules* **1999**, *32*, 6578.

[13] D. Terunuma, R. Nishio, Y. Aoki, H. Nohira, K. Matsuoka, H. Kuzuhara, *Chem. Lett.* **1999**, 565.

[14] I. M. Sanz, J. W. Goodby, *Liq. Cryst.* **1999**, *26*, 1101.
[15] J. Barberá, M. Marcos, J. L. Serrano, *Chem. Eur. J.* **1999**, *5*, 1834.
[16] J. Barberá, M. Marcos, A. Omenat, J. L. Serrano, J. I. Martínez, P. J. Alonso, *Liq. Cryst.* **2000**, *27*, 255.
[17] X. H. Cheng, S. Diele, C. Tschierske, *Angew. Chem.* **2000**, *112*, 605; *Angew. Chem. Int. Ed.* **2000**, *39*, 592.
[18] P. L. Dubin, S. L. Edwards, J.-L. Kaplan, M. S. Mehta, D. A. Tomalia, J. Xia, *Anal. Chem.* **1992**, *64*, 2344.
[19] a) A. Skoulios, D. Guillon, *Mol. Cryst. Liq. Cryst.* **1988**, *165*, 317; b) C. Tschierske, *J. Mater. Chem.* **1998**, *8*, 1485.
[20] a) P. A. Spegt, A. E. Skoulios, *Acta. Crystallogr.* **1966**, *21*, 892; b) P. Weber, D. Guillon, A. Skoulios, *Liq. Cryst.* **1991**, *9*, 369; c) B. Heinrich, K. Praefcke, D. Guillon, *J. Mater. Chem.* **1997**, *7*, 1363; d) B. Donnio, B. Heinrich, T. Gulik-Krzywicki, H. Delacroix, D. Guillon, D. W. Bruce, *Chem. Mater.* **1997**, *9*, 2951; e) F. D. Cukiernik, M. Ibn-Elhaj, Z. D. Chaia, J. C. Marchon, A. M. Giroud-Godquin, D. Guillon, A. Skoulios, P. Maldivi, *Chem. Mater.* **1998**, *10*, 83; f) G. Ungar, D. Abramic, V. Percec, J. A. Heck, *Liq. Cryst.* **1996**, *21*, 73.
[21] A. K. Doolittle, *J. Appl. Phys.* **1951**, *22*, 1471.
[22] a) *International Tables for Crystallography*, *Vol. A*, 4th ed., (Ed.: T. Hahn), International Union of Crystallography, **1995**; b) C. Giacovazzo, H. L. Monaco, D. Viterbo, F. Scordari, G. Gilli, G. Zanotti, M. Catti in *Fundamentals of Crystallography*, (Ed.: C. Giacovazzo), International Union of Crystallography, **1992**.
[23] In the case of a mesomorphic columnar system: a) R. Seghrouchni, A. Skoulios, *J. Phys. II* **1995**, *5*, 1385; b) R. Seghrouchni, A. Skoulios, *J. Phys. II* **1995**, *5*, 1547.
[24] Y. Hendrikx, A. M. Levelut, *Mol. Cryst. Liq. Cryst.* **1988**, *165*, 233.
[25] D. Guillon, *Struct. Bond.* **1999**, *95*, 41.
[26] A first estimation of this geometrical factor has been attempted in: A. Mathis, M. Galin, J. C. Galin, B. Heinrich, C. G. Bazuin, *Liq. Cryst.* **1999**, *26*, 973.

Received: May 2, 2000 [F2455]